Letters

A Misalignment Tolerant IPT System With Intermediate Coils for Constant-Current Output

Ruikun Mai, *Member, IEEE*, Bin Yang, Yang Chen, *Student Member, IEEE*, Naijian Yang, Zhengyou He, *Senior Member, IEEE*, and Shibin Gao

***Abstract*—Misalignment in an inductive power transfer (IPT) system is inevitable for most of the cases, which leads to system performance degradation due to the variation of system parameters. A novel IPT topology with two intermediate coils, one for primary side and the other for secondary one, is proposed to improve an anti-misalignment characteristic. With the merit of the proposed topology, a constant-current output characteristic is achieved, and the system can operate safely without any secondary side. Then, the parameter design and optimization method of the magnetic coupler with intermediate coils are elaborated to improve misalignment performance. Finally, a 3.4-kW experimental setup is built to verify the feasibility of the proposed method. Experimental results show that the four-coil IPT system can tolerate ±225 mm *X*-misalignment, −30 to +50 mm *Y*-misalignment, and −20 to +70 mm *Z*-misalignment with load varying from 40 to 60 Ω, while the fluctuation of the output current is within ±5%. The system efficiency of the IPT system is from 92.1% up to 96.3% with misalignment and variable load (40–60 Ω).**

***Index Terms*—Constant current (CC), intermediate coils, inductive power transfer (IPT) systems, misalignment performance.**

I. Introduction

AN INDUCTIVE power transfer (IPT) technique has been employed in many applications, such as consumer electronics [1], biomedical implant devices [2], underwater power supplies [3], and electric vehicles [4]. It is universal that the primary and pick-up pads of IPT systems are hardly well aligned in practice. Misalignments can change the mutual inductances dramatically, causing instability and reduction in power transfer and efficiency. Therefore, the development of misalignment tolerant IPT systems has drawn much attention from researchers.

In order to enable IPT systems to operate with misalignment tolerance, some control schemes are proposed in [5] and [6]. These methods require closed-loop controllers and RF communication, which increase the complexity and cost of the systems. Control schemes can be simplified if the IPT systems are with an inherent characteristic of misalignment tolerance. Hence, a number of approaches, such as the design of magnetic pads, optimization of compensation parameters, and hybrid topologies, are presented to improve misalignment performance. Some novel magnetic couplers, such as Double-D, bi-polar pads [7], [8], are designed to obtain uniform magnetic field for pick-up pads in one direction. Aiming at combating two- or three-dimensional displacements, parameters of compensation topologies are tuned [9]–[11]. These approaches have no constant output, and some suffer from low efficiency because the input impedance of the inverters is no longer resistive. Moreover, some hybrid topologies, such as S-*LCC*/*LCC*-S [12] and *LCC*-*LCC*/SS [13], are proposed for the sake of efficiency and misalignment tolerance improvement, as well as constant output. However, the primary series compensation has an evident drawback, i.e., the system may be destroyed by the large current and power flowing through primary coil when the coupling coefficient drops to zero, i.e., Fig. 1. In order to overcome the abovementioned issue, Zhao *et al.* [14] use dual-coupled *LCC*-compensated topologies against coupling variations. These methods [12]–[14] utilize some passive components increasing cost of the IPT systems. The third coil is used to improve misalignment tolerance at the cost of compromise in transfer efficiency and mutual inductance of the system [15].

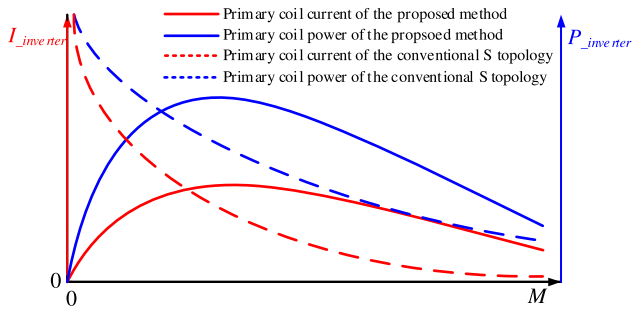

Fig. 1. Output current/power of the inverter versus mutual inductance with different situations.

In this letter, two additional intermediate coils with resonant capacitors are adopted to improve system misalignment tolerant with constant-current (CC) output. Besides, the proposed topology can avoid large current occurrence when the secondary side moves away, which is the main drawback of the S compensation on the primary side. The analysis of the four-coil IPT system is described in Section II. The parameter design and optimization method of the magnetic coupler with intermediate coils are presented in Section III. In Section IV, a 3.4-kW prototype was built to verify the theoretical analysis. Finally, the conclusion is drawn in Section V.

Manuscript received December 1, 2018; revised January 7, 2019; accepted January 28, 2019. Date of publication February 11, 2019; date of current version May 22, 2019. This work was supported in part by the National Natural Science Foundation of China under Grant 51677155, in part by the National Key Research and Development Program of China under Project 2017YFB1201002, in part by the National Science Fund for Distinguished Young Scholars under Grant 51525702, and in part by the Sichuan Youth Science & Technology Foundation (2016JQ0033). *(Corresponding author: Ruikun Mai.)*

The authors are with the School of Electrical Engineering, Southwest Jiaotong University, Sichuan 611756, China (e-mail:

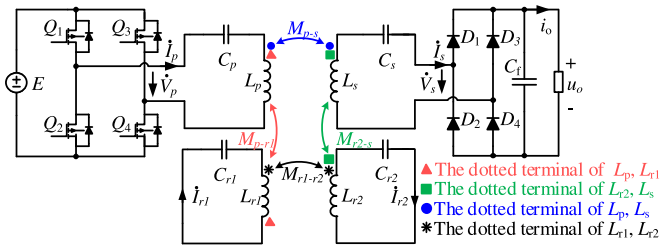

Fig. 2. Proposed IPT system with two additional intermediate coils.

II. Theoretical Analysis

Fig. 2 illustrates the proposed SS four-coil IPT system. The fundamental harmonic approximation method is employed to analyze the compensation topology. Each coil is with the same resonant angle frequency at $\omega = 1/\sqrt{L_P C_P} = 1/\sqrt{L_S C_S} = 1/\sqrt{L_{r2} C_{r2}}$, and parasitic resistances are neglected. Mutual inductances M_{p-r2} and M_{r1-s} are assumed to be small and can be ignored with the coil design. According to Kirchhoff's voltage law, the system can be described as

$$\begin{bmatrix} Z_{p,p} & Z_{p,r1} & Z_{p,r2} & Z_{p,s} \\ Z_{p,r1} & Z_{r1,r1} & Z_{r1,r2} & Z_{r1,s} \\ Z_{p,r2} & Z_{r1,r2} & Z_{r2,r2} & Z_{r2,s} \\ Z_{p,s} & Z_{r1,s} & Z_{r2,s} & Z_{s,s} \end{bmatrix} \begin{bmatrix} \dot{I}_p \\ \dot{I}_{r1} \\ \dot{I}_{r2} \\ \dot{I}_s \end{bmatrix} = \begin{bmatrix} \dot{V}_p \\ 0 \\ 0 \\ 0 \end{bmatrix} \tag{1}$$

where

$$\begin{aligned} &Z_{p,p} = j\omega L_p + 1/j\omega C_p, \quad Z_{p,r1} = -j\omega M_{p-r1}, \\ &Z_{p,r2} = 0 \\ &Z_{p,s} = -j\omega M_{p-s}, \quad Z_{r1,r1} = j\omega L_{r1} + 1/j\omega C_{r1}, \\ &Z_{r1,r2} = -j\omega M_{r1-r2} \\ &Z_{r1,s} = 0, \quad Z_{r2,r2} = j\omega L_{r2} + 1/j\omega C_{r2}, \\ &Z_{r2,s} = j\omega M_{r2-s} \\ &Z_{s,s} = j\omega L_s + 1/j\omega C_s + R_{\mathrm{ac}}. \end{aligned}$$

After solving (1), the currents of each coil are obtained as

$$\begin{cases} \dot{I}_p = \dot{V}_p R_{\mathrm{ac}} M_{r1-r2}^2 / \left[\omega^2 (M_{p-r1} M_{r2-s} + M_{p-s} M_{r1-r2})^2\right] \\ \dot{I}_s = j\dot{V}_p / \left[\omega \left(\frac{M_{p-r1} M_{r2-s}}{M_{r1-r2}} + M_{p-s}\right)\right] \\ \dot{I}_{r1} = -j\dot{V}_p M_{r2-s} / \left[\omega (M_{p-r1} M_{r2-s} + M_{p-s} M_{r1-r2})\right] \\ \dot{I}_{r2} = \dot{V}_p R_{\mathrm{ac}} M_{p-r1} M_{r1-r2} / \left[\omega^2 (M_{p-r1} M_{r2-s} + M_{p-s} M_{r1-r2})^2\right] \end{cases} \tag{2}$$

According to (2), the output current and voltage of the inverter are with the same phase, so zero phase angle (ZPA) can be achieved. The output current I_S is load-independent with the load R_{ac}. When the secondary side moves away, M_{r1-r2} is approaching zero and $\lim_{M_{r1-r2}\to 0, M_{p-s}\to 0} \dot{I}_p = 0$, so that the system can operate without secondary side.

The intermediate coil $r1(r2)$ is mounted on the primary(secondary) side, so the mutual inductance $M_{p-r1}(M_{r2-s})$ of coils L_p, $L_{r1}(L_s, L_{r2})$ can remain constant with misalignment. The product of M_{p-r1} and M_{r2-s} is noted as $A = M_{p-r1} M_{r2-s}$, and the current gain of the system G_{CV} can be calculated as

$$G_{CV} = \left|\frac{\dot{I}_s}{\dot{V}_p}\right| = 1/\left[\omega \left(\frac{A}{M_{r1-r2}} + M_{p-s}\right)\right]. \tag{3}$$

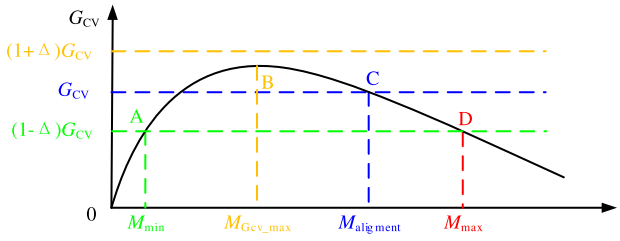

Fig. 3. Profiles of G_{CV} versus mutual inductance, where G_{CV}, Δ, $M_{\mathrm{alignment}}$, M_{min}, and M_{max} are required current gain, deviation of the output current, the minimum mutual inductance, and the maximum mutual inductance, respectively.

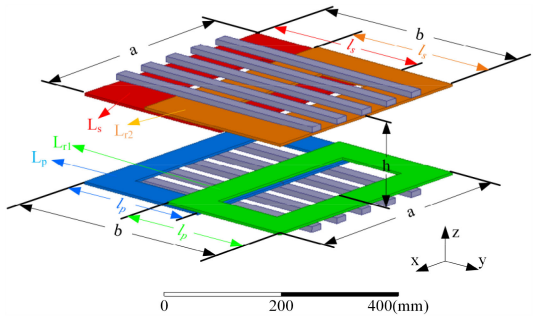

Fig. 4. Structure and dimensions of the magnetic pad.

When the misalignment happens, the mutual inductances M_{p-s} and M_{r1-r2} will decrease or increase simultaneously. If the value of A is designed properly, the current gain G_{CV} can maintain a relatively constant value in a certain range in terms of (3). For simplification, M_{p-s} and $M_{r1-r2}(M = M_{p-s} = M_{r1-r2})$ are assumed to be the same by the proper coil design; (3) can be further simplified as

$$G_{CV} = \left|\frac{\dot{I}_s}{\dot{V}_p}\right| = 1/\left[\omega \left(\frac{A}{M} + M\right)\right]. \tag{4}$$

The relationship between G_{CV} and M is shown in Fig. 3, from which we can derive

$$\begin{cases} M_{\mathrm{alignment}} = \left(\sqrt{1 - 4A\omega^2 {G_{CV}}^2} + 1\right) / (2\omega G_{CV}) \\ M_{\mathrm{min}} = \left(1 - \sqrt{1 - 4A(1-\Delta)^2 \omega^2 {G_{CV}}^2}\right) / (2(1-\Delta)\omega G_{CV}) \\ M_{\mathrm{max}} = \left(1 + \sqrt{1 - 4A(1-\Delta)^2 \omega^2 {G_{CV}}^2}\right) / (2(1-\Delta)\omega G_{CV}) \\ M_{G_{CV}\_\mathrm{max}} = \sqrt{A} \end{cases} \tag{5}$$

When M equals M_{Gcv_max}, the current gain can reach the maximum value, so we have

$$A \geq 1/\left[4(1+\Delta)^2 \omega^2 |G_{CV}|^2\right]. \tag{6}$$

III. Design of Magnetic Coupler

In order to obtain required magnetic coupler, ANSYS MAXWELL is used to assist to design. The structure and dimensions of the magnetic pad are shown in Fig. 4. Ferrite bars are attached to the corresponding coil. The flowchart for the design of magnetic coupler is illustrated in Fig. 5.

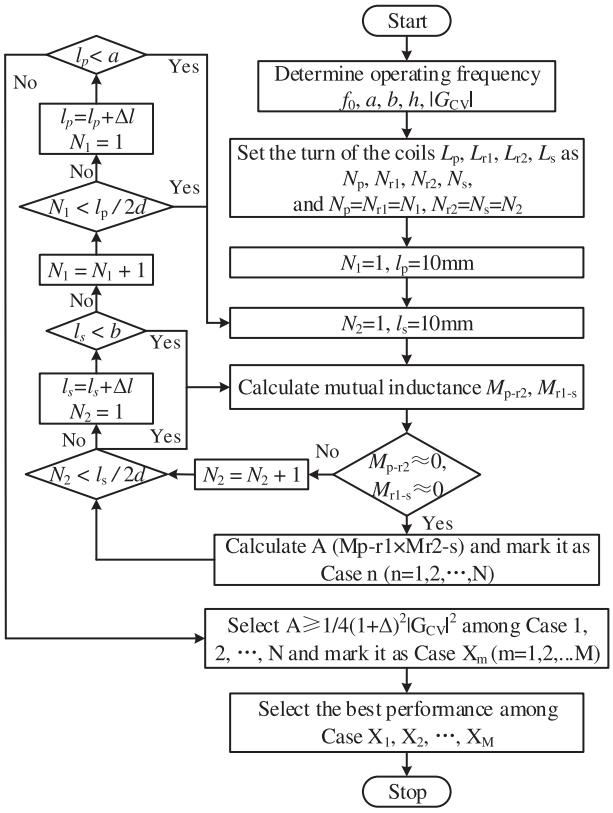

Fig. 5. Flowchart for the design of the magnetic pad, where d and Δl are the diameter of litz wire and step size of the coil, respectively. Case X_m ($n = 1, 2, \ldots, M$) represent all the magnetic pads that satisfy $M_{p-r2} \asymp 0$, $M_{r1-s} \asymp 0$, and $A \geq 1/4(1+\Delta)^2|G_{CV}|^2$.

An instant of the magnetic coupler is designed as follows. Parameters are given as: operating frequency $f_0 = 85$ kHz, coil size $a = 450$ mm, $b = 450$ mm, air gap $h = 150$ mm, current gain $|G_{CV}| = 2.28\%$, diameter of litz wire $d = 4.2$ m, step size $\Delta l = 25$ mm, and deviation of the output current $\Delta = 5\%$. After simulation, the results are $l_p = 260$ mm, $l_s = 310$ mm, $N_p = 15$, and $N_s = 25$. The simulated mutual inductances versus X-, Y-, and Z-misalignment are shown in Fig. 6, which indicate that the proposed mutual inductances M_{p-r2} and M_{r1-s} of magnetic coupler can be ignored in X- and Z-misalignment, while these two mutual inductances cannot be neglected with the occurrence of Y-misalignment so that the system cannot have large misalignment with the proposed method.

IV. Experimental Results

In order to demonstrate the applicability of the proposed method, a 3.4-kW experimental prototype was built as shown in Fig. 7. The switching devices are Q_1–Q_4 = C2M0080120D and D_1–D_4 = GP2D050A120B. System parameters are listed in Table I. An electronic load (IT8816B) is used to verify the performance of the CC output.

Fig. 8(a) and (b) shows the experimental waveforms of the output current/voltage of the inverter and input current/voltage of the rectifier at $R = 60\,\Omega$ with a 150-mm gap in different situations of X-misalignment. Fig. 8(c) and (d) shows the experimental waveforms at $R = 60\ \Omega$ in different situations of Z-misalignment. ZPA can be realized both in well-aligned case and as in X-misaligned and Z-misaligned cases.

Fig. 9(a) illustrates the output current of the four-coil IPT system versus misalignment and load. With 225 mm (50%) X-misalignment,

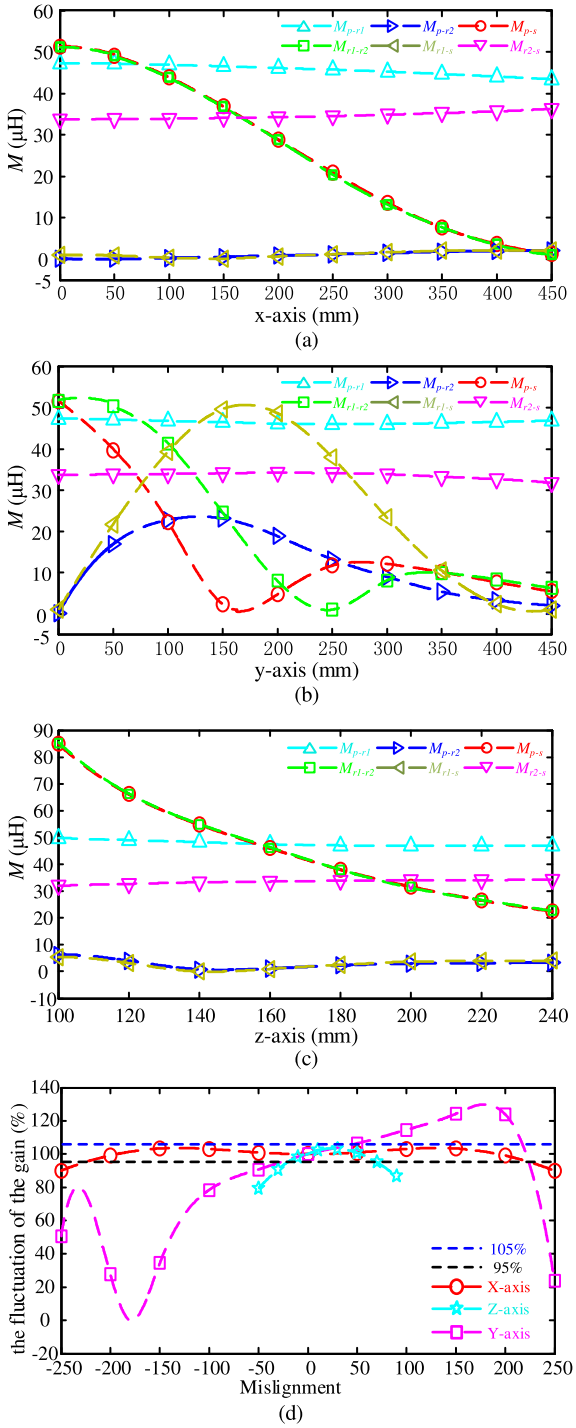

Fig. 6. Variation of mutual inductances due to misalignment of secondary pads in (a) X-, (b) Y-, (c) Z-axis and (d) the fluctuation of the current gain of the system G_{GV} with misalignment of secondary pads in the X-, Y-, and Z-axis.

the fluctuation of the output current is less than 4.4% while the load changing from 40 to 60 Ω. The results demonstrate that the system has good X-misalignment and CC output performance. The corresponding efficiencies are measured as shown in Fig. 9(b). The system efficiency of the IPT system is from 92.2% up to 96.2% with misalignment and variable load.

Fig. 10(a) explains that the air gap of the system can increase to 220 mm or decrease to 130 mm, and the deviation of the output current

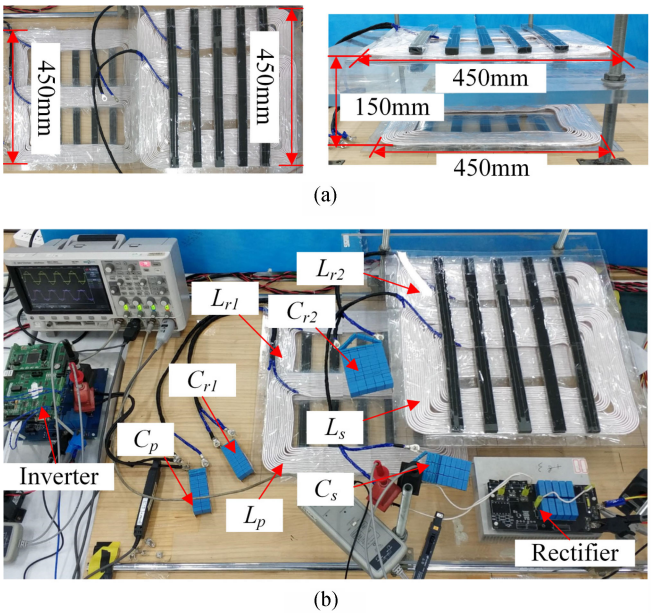

Fig. 7. (a) Structure of coil pads. (b) Setup of the four-coil IPT system.

TABLE I
SYSTEM SPECIFICATION AND PARAMETER VALUES

Parameter	value	Parameter	value	Parameter	value
E	410 V	i_o	7.5 A	Δ	5%
f	85 kHz	$M_{\text{p-s}}$	51.62 μH	$M_{\text{r1-r2}}$	51.77 μH
$M_{\text{p-r1}}$	47.29 μH	$M_{\text{r2-s}}$	33.15 μH	$M_{\text{p-r2}}$	0.08 μH
$M_{\text{r1-s}}$	0.06 μH	L_{p}	159.41 μH	L_{r1}	165.85μH
C_{p}	21.92 nF	C_{r1}	21.04 nF	L_{r2}	330.51 μH
L_{s}	355.11 μH	C_{r2}	10.57 nF	C_{s}	9.84 nF

is still within ±5%. The experimental results verify that the system also has great *Z*-misalignment with the CC output. Besides, the efficiency of the IPT system is from 92.1% up to 96.3% with *Z*-misalignment and variable load as shown in Fig. 10(b).

As for misalignment in the *Y*-axis, similar experiments are also observed. The designed IPT system can only tolerate maximum lateral misalignment to 50 mm with a 5% deviation. The reason for that is mutual inductance M_{p-r2} and M_{r1-s} cannot be neglected with *Y*-misalignment.

In order to further verify the CC output characteristic of the proposed approach, two load step-changes are conducted in the experiment shown in Fig. 11(a). At first, the resistive load of the electronic load alters from 20 to 40 Ω, and then back to 20 Ω. The output currents i_o of the two moments are with a minor difference (7.62 A for 20 Ω and 7.57 A for 40 Ω). It can be seen that the percentage of load change is 100% and that of current change is only 0.66%, resulting from parameter errors of inductor and capacitors. However, compared with the change of load, the change of output current is quite small. Therefore, the output current of the proposed converter system can be approximately treated as CC.

In order to further verify that the proposed approach can operate safely without any secondary side, the secondary side is removed (M_{p-s} and M_{r1-r2} are close to zero) in the experiment as shown in Fig. 11(b). It indicates that the current in primary coil and output current are nearly zero. Thus, the system can operate safely without the secondary side.

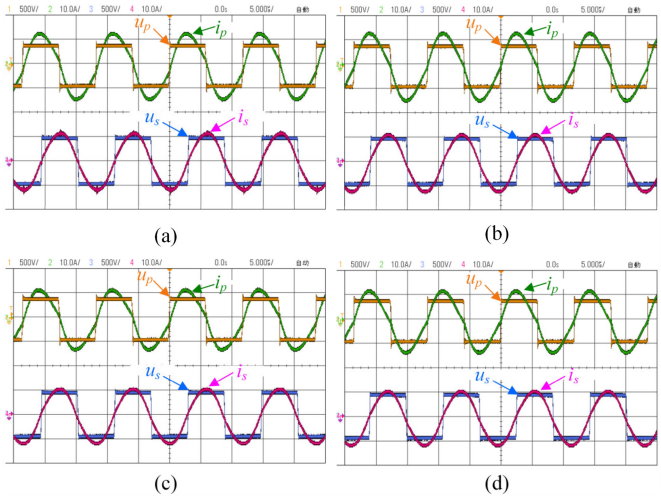

Fig. 8. Experimental waveforms of v_P, i_P, v_S, i_S at $R = 60\ \Omega$. (a) In well-aligned case. (b) With 225 mm *X*-misalignment. (c) With −20 mm *Z*-misalignment. (d) With 70 mm *Z*-misalignment.

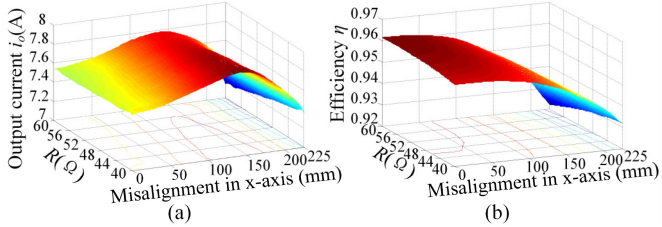

Fig. 9. Measured output current and efficiencies versus *R* and *X*-misalignment.

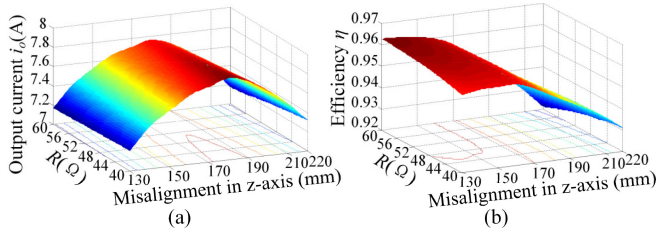

Fig. 10. Measured output current and efficiencies versus *R* and *Z*-misalignment.

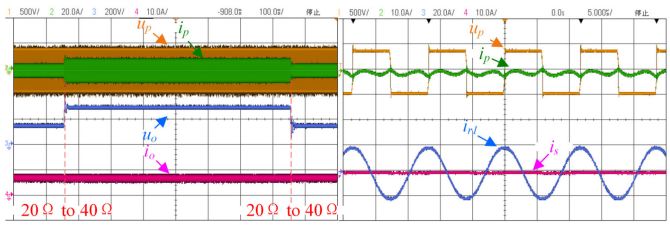

Fig. 11. (a) Experimental waveforms when sudden load change happens. (b) Experimental waveforms when the secondary side moves far away (mutual inductances M_{p-s} and M_{r1-r2} are zero).

V. CONCLUSION

An IPT system with two intermediate coils is proposed to improve misalignment tolerance with the CC output. Besides, it can limit the exponential increase in the primary current when the secondary side is not presented. Parameter and magnetic coupler are optimized in detail to

obtain high-misalignment tolerance. Experimental results demonstrate that the four-coil IPT system can confine the output current variation less than 5% with load varying from 40 to 60 Ω when the secondary side is misaligned from −225 to 225 mm along the *X*-axis, −30 to 50 mm along the *Y*-axis, and −20 to 70 mm along the *Z*-axis. Moreover, the maximum efficiency can reach 96.3% with a 130-mm gap in a well-aligned case. The proposed approach is suitable for the charging applications with rails, such as modern tram logistics robot.

In the future, the misalignment performance in the *Y*-axis of the four-coil system is required to be improved.

REFERENCES

[1] S. Y. Hui, "Planar wireless charging technology for portable electronic products and Qi," *Proc. IEEE*, vol. 101, no. 6, pp. 1290–1301, Jun. 2013.

[2] A. K. RamRakhyani, S. Mirabbasi, and C. Mu, "Design and optimization of resonance-based efficient wireless power delivery systems for biomedical implants," *IEEE Trans. Biomed. Circuits Syst.*, vol. 5, no. 1, pp. 48–63, Feb. 2011.

[3] H. Fukuda, N. Kobayashi, K. Shizuno, S. Yoshida, M. Tanomura, and Y. Hama, "New concept of an electromagnetic usage for contactless communication and power transmission in the ocean," in *Proc. IEEE Int. Underwater Technol. Symp.*, Tokyo, Japan, 2013, pp. 1–4.

[4] W. Y. Lee, J. Huh, and S. Y. Choi, "Finite-width magnetic mirror models of mono and dual coils for wireless electric vehicles," *IEEE Trans. Power Electron.*, vol. 28, no. 13, pp. 1413–1428, Mar. 2013.

[5] F. F. Van Der Pijl, M. Castilla, and P. Bauer, "Adaptive sliding-mode control for a multiple-user inductive power transfer system without need for communication," *IEEE Trans. Ind. Electron.*, vol. 60, no. 1, pp. 271–279, Jan. 2013.

[6] M. J. Neath, A. K. Swain, U. K. Madawala, and D. J. Thrimawithana, "An optimal PID controller for a bidirectional inductive power transfer system using multiobjective genetic algorithm," *IEEE Trans. Power Electron.*, vol. 29, no. 3, pp. 1523–1531, Mar. 2014.

[7] M. Budhia, J. T. Boys, G. A. Covic, and C.-Y. Huang, "Development of a single-sided flux magnetic coupler for electric vehicle IPT charging systems," *IEEE Trans. Ind. Electron.*, vol. 60, no. 1, pp. 318–328, Jan. 2013.

[8] A. Zaheer, G. A. Covic, and D. Kacprzak, "A bipolar pad in a 10-kHz 300-W distributed IPT system for AGV applications," *IEEE Trans. Ind. Electron.*, vol. 61, no. 7, pp. 3288–3301, Jul. 2014.

[9] H. Feng, T. Cai, S. Duan, X. Zhang, H. Hu, and J. Niu, "A dual-side-detuned series–series compensated resonant converter for wide charging region in a wireless power transfer system," *IEEE Trans. Ind. Electron.*, vol. 65, no. 3, pp. 2177–2188, Mar. 2018.

[10] J. Zhao, T. Cai, S. Duan, H. Feng, C. Chen, and X. Zhang, "A general design method of primary compensation network for dynamic WPT system maintaining stable transmission power," *IEEE Trans. Power Electron.*, vol. 31, no. 12, pp. 8343–8358, Dec. 2016.

[11] F. Lu, H. Zhang, H. Hofmann, W. Su, and C. C. Mi, "A dual-coupled LCC-compensated IPT system with a compact magnetic coupler," *IEEE Trans. Power Electron.*, vol. 33, no. 7, pp. 6391–6402, Jul. 2018.

[12] Y. Chen, B. Yang, Z. Kou, Z. He, G. Cao, and R. Mai, "Hybrid and reconfigurable IPT systems with high-misalignment tolerance for constant-current and constant-voltage battery charging," *IEEE Trans. Power Electron.*, vol. 33, no. 10, pp. 8259–8269, Oct. 2018.

[13] L. Zhao, D. J. Thrimawithana, and U. K. Madawala, "Hybrid bidirectional wireless EV charging system tolerant to pad misalignment," *IEEE Trans. Ind. Electron.*, vol. 64, no. 9, pp. 7079–7086, Sep. 2017.

[14] L. Zhao, D. J. Thrimawithana, U. K. Madawala, P. Hu, and C. C. Mi, "A misalignment tolerant series-hybrid wireless EV charging system with integrated magnetics," *IEEE Trans. Power Electron.*, vol. 34, no. 2, pp. 1276–1285, Feb. 2019, doi: 10.1109/TPEL.2018.2828841.

[15] Y. Chen, R. Mai, Y. Zhang, M. Li, and Z. He, "Improving misalignment tolerance for IPT system using a third-coil," *IEEE Trans. Power Electron.*, to be published, doi: 10.1109/TPEL.2018.2867919.